Supplementary Materials

Large-scale fabrication, 3D tomography, and lithium-ion battery application of porous silicon

Mingyuan Ge[1], Yunhao Lu[2], Peter Ercius[3], Jiepeng Rong[1], Xin Fang[1], Matthew Mecklenburg[4] and Chongwu Zhou[1]

[1]Department of Electrical Engineering and Department of Chemical Engineering and Materials Science, University of Southern California, Los Angeles, CA 90089

[2]Department of Materials Science and Engineering Zhejiang University, Hangzhou, Zhejiang 310027, P. R. China

[3]National Center for Electron Microscopy, Lawrence Berkeley National Laboratory, Berkeley, CA 94720, USA

[4]Center for Electron Microscopy and Microanalysis, University of Southern California, Los Angeles, CA 90089

- **Fe and Al concentration in ball-milled metallurgical Si**

Iron (Fe) and aluminum (Al) are the two major impurities. To determine their concentration in metallurgical silicon after ball milling, 0.5 g sample was put into polytetrafluoroethene (PTFE) beaker containing 5 ml concentrated nitric acid (HNO_3). 5 ml hydrofluoric acid (HF, 50 wt. %) was then added by droplets to dissolve the

sample to get a clear solution. The solution was added with additional 5 ml acid mixture (sulfuric acid (H_2SO_4): phosphorous acid (H_3PO_3) = 3 : 2 by volume) and kept at 130 ^oC for 5 min. At this stage, all the silicon was converted to silicon tetrafluoride (SiF_4) and removed by volatilization, leaving only boron in the solution. The solution was then cooled down, and diluted with DI water. Fe and Al concentration measurements were performed using HORIBA Jobin Yvon ULTIMA-C inductively coupled plasma emission spectrometer (ICP-AES). After ball-milling, atomic percentage of Fe and Al in silicon powder are 1.9% and 0.47%, respectively. The feature size of the silicon powder after ball-milling is around 1 μm, as shown in Figure S1.

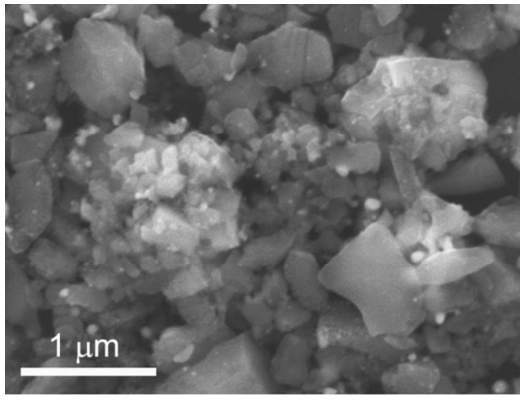

Figure S1. SEM image of silicon powder after ball-milling.

- **Pore size distribution of porous (Si(1))**
-

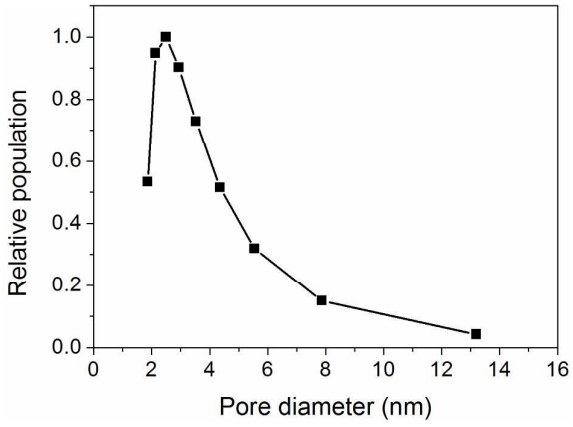

Figure S2. Pore size distribution of porous **Si(1)**

- **X-ray diffraction of porous Si(1)**

  Coherent domain size can be calculated using Scherrer formula, which gives a average domain size of 19 nm. Figure S3 shows the XRD pattern of porous **Si(1)**.

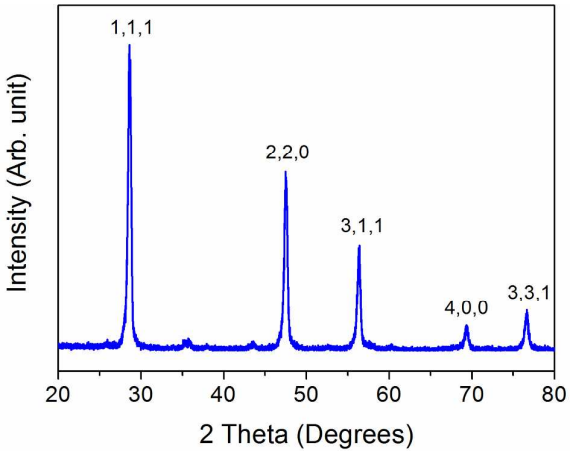

Figure S3. XRD pattern of porous **Si(1)**

- **First principle calculation**

First-principle calculations were performed using the VASP code[1]. The ultrasoft peusdo-potentials were used to model electron–ion interactions. Structure relaxation was carried out using the generalized gradient approximation (GGA) for exchange-correlation function[2]. The k-space integration was done by summing over the Monkhorst-Pack special points in the Brillouin zone. The Gaussian method, with a smearing width of 0.05eV was used in determination of the Fermi level. The plane wave basis set was restricted by cutoff energy of 425 eV. Defect calculations were performed using 3x3x3 supercells corresponding to ~0.5% defect concentration, and 2x2x2 k-point mesh was used for total energy calculations. The forces acting on the relaxed atoms are <0.02 eV/Å in the optimized structures.

- **Reactions between $Fe(NO_3)_3$ and Si:**

Both Fe^{3+} and NO_3^- can oxidize Si. The reaction between Fe^{3+} and Si is shown as:

$$4Fe^{3+} + Si + 6F^- \rightarrow 4Fe^{2+} + [SiF_6]^{2-}$$

However, NO_3^- has a complex behavior in the acidic environment (in the present of HF):

$$NO_3^- + H^+ \leftrightarrow HNO_3$$
$$H^+ + NO_2^- + HNO_3 \rightarrow 2NO_2 + H_2O$$
$$2NO_2 + Si \rightarrow Si^{2+} + 2NO^{2-}$$
$$Si^{2+} + 2(OH)^- + 6HF \rightarrow H_2SiF_6 + H_2O + H_2$$

According to the Nernst equation: $E = E^0 + \frac{RT}{nF} \ln \frac{a_{ox}}{a_{red}}$, increase of $[H^+]$ concentration will increase the oxidation potential.

- **Morphology of Si(1), Si(3) and Si etched with additional HNO_3**

Another control experiment was conducted to help to identify the role that NO_3^- played in the etching process. In the experiment, similar to the etch condition as for **Si(1)**, $Fe(NO_3)_3$ was reduced by 20% and replaced by HNO_3 to keep total concentration of NO_3^- a constant. This sample is denoted as **Si(3)**. Figure S4 compares the morphology of **Si(1)** and **Si(3)** using SEM and TEM. The structure of the two samples is very similar, and both of them clearly show the porous feature. The specific surface area of **Si(3)** is 80 m^2/g, quite comparable to the surface area of **Si(1)** which is 70 m^2/g.

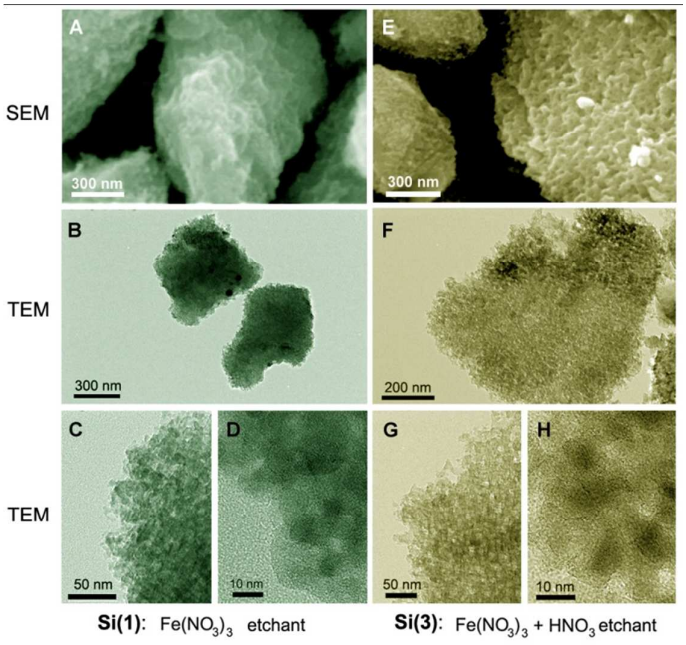

Figure S4. Morphology comparison (SEM images: **a** and **e**, TEM images: the rest) of porous silicon etched using different etchant. **a**-**d**: SEM and TEM images of **Si(1)** (etched in $Fe(NO_3)_3$/HF)**,** which show the highly porous structure of the particles, and

individual pores can be discerned from high-magnification TEM images (e.g. **D**). **e**-**h**: SEM and TEM images of **Si(3)** (etched in $Fe(NO_3)_3/HNO_3/HF$), which show similar structure to **Si(1)**.

- **Etching on undoped Si**

Silicon nanoparticles bought from Alfa were etched under the same condition as for **Si(1)**. Figure S5 shows that the particles remained solid without any formation of porous structure, which demonstrates that impurities in silicon play a pivotal role in obtaining porous silicon.

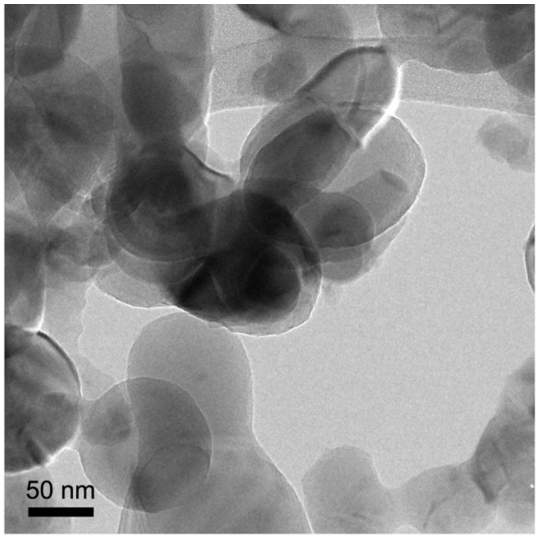

Figure S5. TEM image of undoped silicon nanoparticles after etching, which remained solid structure without formation of pores.

- **Tap density of porous silicon electrode**

Tap density is estimated by measuring weight and volume of the active material on the substrate. The electrode has a surface area of 1.5 cm^2 and a thickness of 10 μm (Figure S6). The tap density is determined to be about 0.54 g/cm^3 for silicon in the electrode.

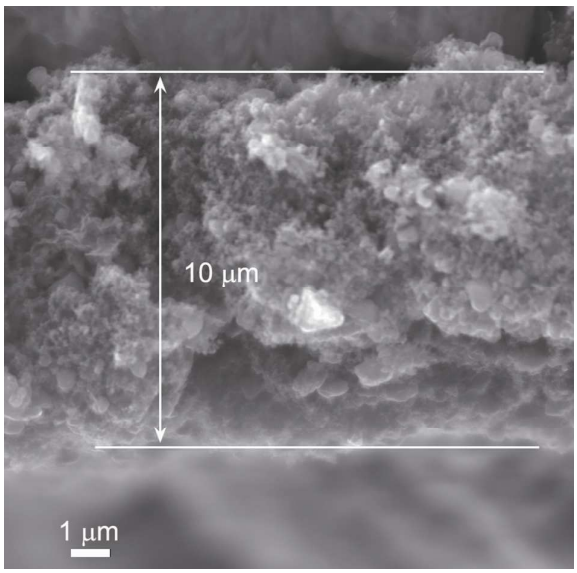

Figure S6. Side view of electrode showing the thickness of active material layer is around 10 μm

- **Nano-indentation on porous silicon particles**

A multimode AFM (Veeco Nanoscope IV) was used to carry out the imaging and force-indentation experiment in the tapping mode. The silicon substrate was used as reference to determine the optical sensitivity. The AFM probes used for measurement were silicon probes with spring constant k=40 Nm^{-1} and a tip radius of 25 nm. The force indentation was fitted with Hertz model to determine the Young's modulus[3]. Figure S7 shows the morphology of **Si(1)** before and after indentation.

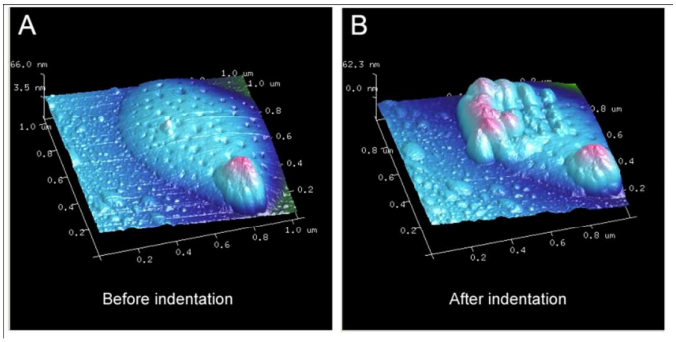

Figure S7. Morphology characterization of a porous silicon particle (**Si(1)**) before (**a**) and after (**b**) indentation using an AFM tip. The protrusion found on the surface after indentation (**b**) indicates the plastic-like deformation of the porous structure.

- **3D tomography and structure characterization**

For 3D tomography, HAADF-STEM images were taken at TECNAI F20 in the National Center for Electron Microscopy at the Lawrence Berkeley Laboratory. HAADF-STEM images were recorded at single rotation from -75^{o} to 75^{o} at 1^{o} interval. A total of 151 images were aligned using ETOMO to reconstruct the 3D structure of particles. Other STEM and TEM images were recorded at JEOL 2100F at Center for Electron Microscopy and Micro Analysis at the University of Southern California. Figure S8 shows the STEM (reprinted from Figure 1C) of porous Si particles and 3D reconstructions.

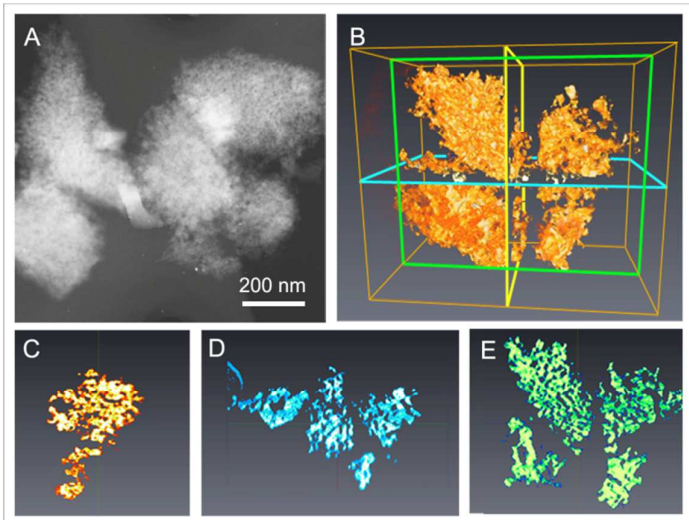

Figure S8. a. A STEM image of porous silicon particles (reprinted from Figure 1C from main text). **b**. Reconstructed structure of the particles from HAADF-STEM 3D tomography. **c-e**. Projected views of orthogonal slices cut through the center of the particle.

- **Electrode fabrication**

Porous silicon particles (**Si(1)**, **Si(2)**) were first coated with carbon using C_2H_4 as gas source and Ar as carrier gas under 860 ^{o}C for 10 minutes. Graphene oxide (GO) was then mixed with particles in water solution, followed by reduction using hydrazine at 90 ^{o}C for 20 minutes. Thermal annealed samples were made by annealing the samples at 700 ^{o}C using H_2 (5% diluted in Ar) as carrier gas for 20 minutes. The porous silicon

electrodes were fabricated by pasting the slurry (Si : carbon-black : alginic acid sodium salt = 7 : 2 : 1 by weight) on a copper foil and then dried at 90 ^{o}C for 6 hours. Later, coin cells were assembled using a lithium foil as the counter/reference electrode; 1 M $LiPF_6$ in dimethyl carbonate / fluoroethylene carbonate (1 : 1 by volume) was used as electrolyte.

- **Elemental mapping of Li and Si**

Figure S9 shows the elemental mapping of Li and Si at lithiated stage for **Si(1)** (the same sample as the one used in Figure 4d in the main text). EELS spectrum is collected under HAADF-STEM. The red and green colors in Figure S4A are denoted for Si and Li, respectively. Figure S4b-d are the EELS spectra corresponding to the square region shown in Figure S9a. Energy losses in range of 57-70 eV are signals related to Li, while energy losses in range of 99-110 eV are signals related to Si. It is found that in region B and C, Li has much higher EELS signal and Si has almost no signal compared with which is shown in region D, indicating the formation of solid-electrolyte interface (SEI).

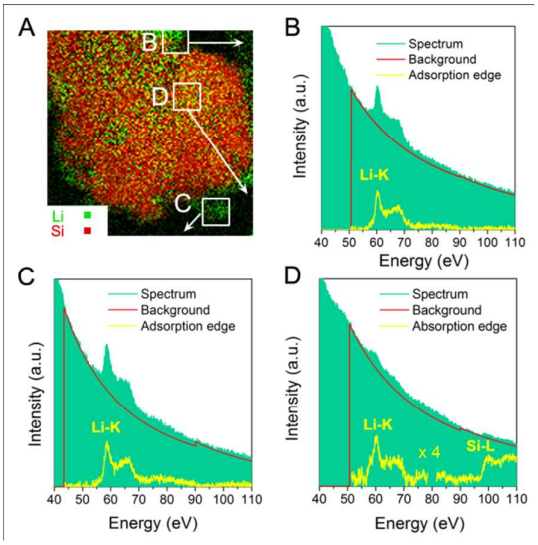

Figure S9. a. EELS mapping of Li (green) and Si (red) at the enlarged region of Figure 4d (in the main text). **b-d**. EELS spectra corresponding to the position shown in **a**. The lithium-rich regions at position A and C indicate the formation of SEI layer.

- **Voltage profile of Si(1) with carbon and GO coating**

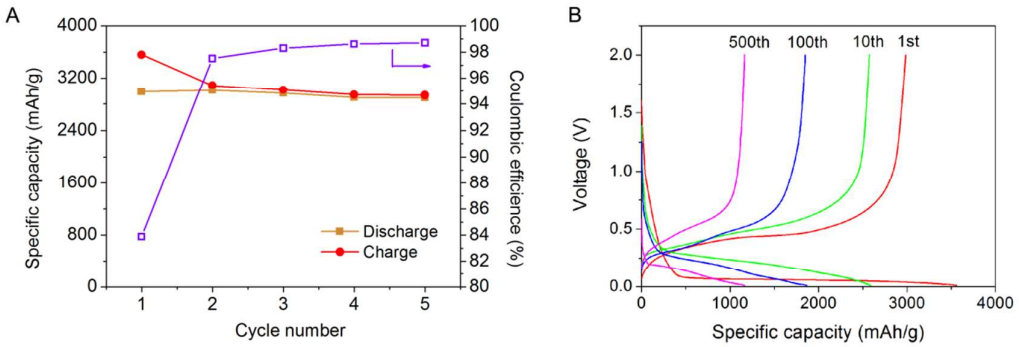

Figure S10. a. Specific capacity and Coulombic efficiency of the first 5 cycles of **Si(1)**. **b**. Voltage profile of **Si(1)** with carbon and GO coating for the 1st, 10th, 100th, and 500th cycle.

- **Etching Si nanoparticles into porous structure**

Silicon nanoparticles were first doped with boron following the method reported previously[4]. 0.2 g as-prepared boron-doped silicon nanoparticle was immersed in the etchant containing 5 M HF and 1.5 mM $Fe(NO_3)_3$ in H_2O. Ethanol was added to suppress the foam formation. The reaction was kept under stirring for 30 min, and then washed for characterization. Figure S11 shows the TEM image of porous silicon nanoparticles at different magnifications.

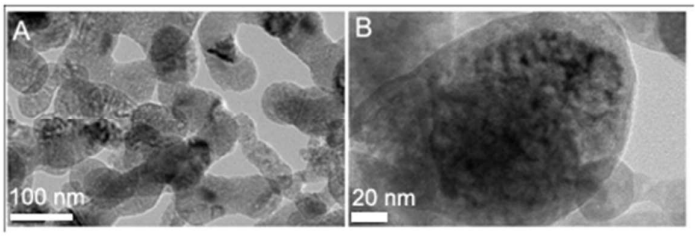

Figure S11. TEM images of porous silicon particles prepared through stain etching on boron-doped silicon nanoparticles.

References

1. Kresse, G.; Furthmuller, J., Efficient iterative schemes for ab initio total-energy calculations using a plane-wave basis set. *Phys Rev B* **1996,** *54* (16), 11169-11186.

2. Perdew, J. P.; Chevary, J. A.; Vosko, S. H.; Jackson, K. A.; Pederson, M. R.; Singh, D. J.; Fiolhais, C., Atoms, Molecules, Solids, and Surfaces - Applications of the Generalized Gradient Approximation for Exchange and Correlation. *Phys Rev B* **1992,** *46* (11), 6671-6687.

3. Sneddon, I. N., The relation between load and penetration in the axisymmetric boussinesq

problem for a punch of arbitrary profile. *International Journal of Engineering Science* **1965,** *3* (1), 47-57.

4. Ge, M. Y.; Rong, J. P.; Fang, X.; Zhou, C. W., Porous Doped Silicon Nanowires for Lithium Ion Battery Anode with Long Cycle Life. *Nano Lett* **2012,** *12* (5), 2318-2323.